Sea Ice Sensing From GNSS-R Data Using Convolutional Neural Networks

Qingyun Yan, *Student Member, IEEE*, and Weimin Huang, *Senior Member, IEEE*

***Abstract*— In this letter, a scheme that uses convolutional neural networks (CNNs) is proposed for sea ice detection and sea ice concentration (SIC) prediction from TechDemoSat-1 Global Navigation Satellite System Reflectometry delay-Doppler maps (DDMs). Specifically, a classification-orientated CNN was designed for sea ice detection and a regression-based one for SIC estimation. Here, DDM images were used as input, and SIC data from Nimbus-7 Scanning Multi-Channel Microwave Radiometer and Defense Meteorological Satellite Program Special Sensor Microwave Imager-Special Sensor Microwave Imager/Sounder sensors were modified as targeted output. In the experimental phase, the CNN output resulted from inputting full-size DDM data (128-by-20 pixels) showed better accuracy than that of the existing NN-based method. Besides, both CNNs and NNs with further processed input data (40-by-20 pixels, and with a fixed position in each image) were evaluated and the performance of both networks was enhanced. It was found that when DDM data are adequately preprocessed, CNNs and NNs share similar accuracy; otherwise the former outperforms the latter. Further conclusion was thus drawn that CNNs were more tolerant to the data format changes than NNs.**

***Index Terms*— Convolutional neural network (CNN), delay-Doppler map (DDM), Global Navigation Satellite System-Reflectometry (GNSS-R), sea ice concentration (SIC), sea ice detection, TechDemoSat-1 (TDS-1).**

I. Introduction

AS AVERAGE sea ice cover has decreased in the North, shipping and offshore operations in these regions have grown steadily [1]. Thus, a good knowledge of sea ice is essential for managing and protecting activities in such areas. Because of a higher and faster coverage, obtaining sea ice information via remote sensing techniques can be more efficient and cost-effective than using *in situ* measurements.

With millions of available TechDemoSat-1 (TDS-1) delay-Doppler maps (DDMs), great interest has been raised in sea ice remote sensing within Global Navigation Satellite System Reflectometry (GNSS-R) circles [2]–[7]. The primary TDS-1 data-based sea ice detection was investigated in [2]. DDMs collected over sea ice were found to be less spread than those over seawater, and for this reason, the quantity of DD pixels that had high normalized values in a DDM was regarded as the detection criterion [2]. This letter was later extended by Zhu *et al.* [3], in which the difference between two adjacent DDMs was computed, and its associated pixel number was derived. The transitions (such as water-water, water-ice, ice-ice, and ice-water) can be classified based on the pixel number. In [4], the coherence (that is characteristic for a surface with large flat areas) in a DDM or a waveform was evaluated for verifying the presence of sea ice. The recognition of sea ice transition based on the scattering coefficient retrieval was proposed in [5]. A perspective of altimetric measurements of the ice sheet cover using DDM data was presented in [6]. In [7], a neural network (NN)-based method was developed for sea ice concentration (SIC) that is the percentage of sea ice-covered area within a given region estimation from DDMs.

Recently, deep learning (DL) has been widely recognized as an excellent technique that could be the new tendency in the development of remote sensing image processing [8] because it is able to learn representations of features exclusively from the data. Furthermore, convolutional NNs (CNNs) have surpassed most DL algorithms in visual recognition [8]. CNN has been successfully applied to sea ice remote sensing using synthetic aperture radar [9] and altimeter [10] data. However, to the best of our knowledge, the application of CNN in GNSS-R area has not yet been conducted. Although good accuracy has been achieved for sea ice remote sensing from GNSS-R DDM using NN [7], it is believed that CNN will perform even better as it takes advantage of the original data format (2-D) instead of 1-D by NN.

In this letter, the CNN technique is applied to TDS-1 DDMs for the first time, dedicated to detecting sea ice and estimating SIC. The CNN for sea ice detection is devised with a classification layer, whereas a regression layer for SIC estimation. The outline of this letter is as follows. The design of CNN-based sea ice remote sensing is described in Section II. Results and analyses are presented in Section III, followed by the conclusions in Section IV.

II. Design of CNN-Based Sea Ice Remote Sensing

A CNN is able to establish the intrinsic connection between input–target pairs when they are well associated [8]. Typically, it consists of a block of optional convolution layers, pooling layers, nonlinear layers, fully connected layers, followed by an output layer. A convolution layer consists of a certain number of filters of a specific size. Each filter can be regarded as a feature extractor and it convolves with the input image. The convolved images are then processed by an activation function (nonlinear layer) to produce feature maps that are the output of the convolution layer. A pooling layer subsamples

Manuscript received February 19, 2018; revised April 28, 2018 and June 13, 2018; accepted June 28, 2018. Date of publication July 23, 2018; date of current version September 26, 2018. The work of W. Huang was supported by the Natural Sciences and Engineering Research Council of Canada Discovery under Grant NSERC RGPIN-2017-04508 and Grant RGPAS-2017-507962. *(Corresponding author: Weimin Huang.)*

The authors are with the Faculty of Engineering and Applied Science, Memorial University, St. John's, NL A1B 3X5, Canada (e-mail: qy2543@mun.ca; weimin@mun.ca).

Color versions of one or more of the figures in this letter are available online at http://ieeexplore.ieee.org.

Digital Object Identifier 10.1109/LGRS.2018.2852143

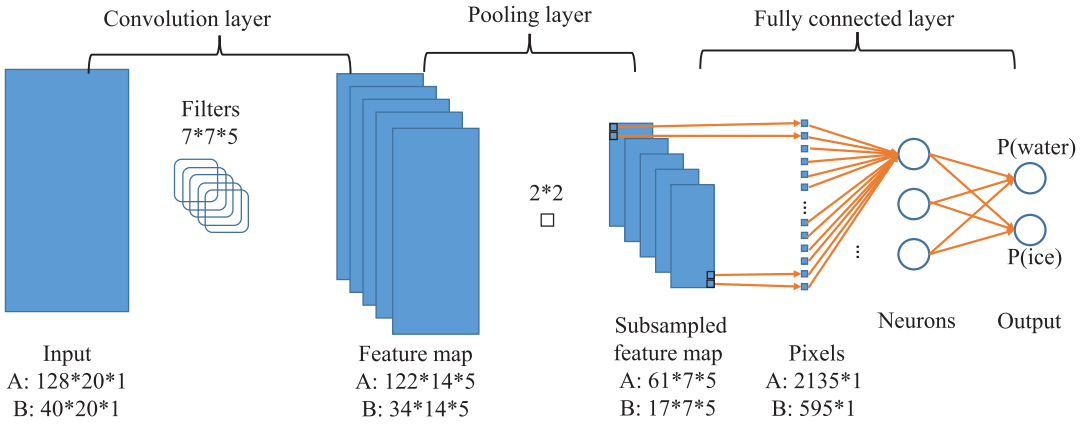

Fig. 1. Employed CNN structure in this letter. Set A parameters are associated with full DDM input and set B for cropped input.

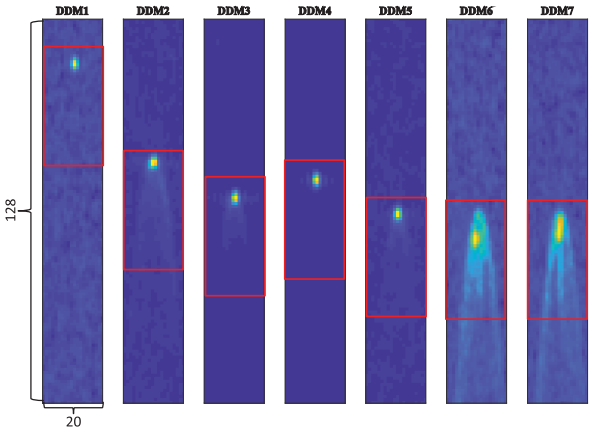

Fig. 2. DDM samples in its original data format (128 × 20), note that their specular points are not aligned. Red boxes: cropped inputs (40 × 20) with settled position within each frame, following the fashion in [7]. Delay axes are in vertical and Doppler axes in horizontal.

the feature map to reduce its redundancy and the output of the last pooling layer is converted to a vector, which is followed by one or more fully connected layers. The fully connected layer combines all of the features learned through the previous layers to identify the desired patterns. Fig. 1 illustrates an example of CNN. The filter parameters in the convolution layer and weights in the fully connected layer are learned through a training process.

A DDM describes the scattering strength of the GNSS-R signal off the observed surface. Each DD pixel corresponds to its associated spatial clusters and this allows the fusion of pixel with other data [11], e.g., SIC in this letter. For this reason, CNN is applied for sea ice detection and SIC prediction from DDM data. CNN applications generally include the following stages: 1) data (DDM in this letter) preprocessing; 2) training of CNN; and 3) testing of CNN using DDMs that are separate from training data.

A. Preprocessing of DDM Images

The preprocessing of DDM data follows the procedures in [7]. Specifically, it consists of noise floor subtraction, normalization, and (optional) signal box determination (see more details in [7]). It should be noted that the positions of DDM specular points are not aligned in all the images (see Fig. 2 for demonstration) due to variation in the path length [12]. The last step is thus necessary for NN so that the input is presented to the network in order [7]. However, it is believed that CNN is able to extract the features independent of DDM's position. Therefore, to demonstrate this, two different CNN structures, which employ full (128-by-20 pixels) and cropped (40-by-20 pixels, the adopted signal box in [7]) DDM images as input, respectively, are devised.

B. Structure of CNN

The framework of the employed CNN for sea ice detection is presented in Fig. 1 (parameters of set A are for full DDM and set B for cropped data). It contains one convolution layer followed by one pooling layer and two fully connected layers. The convolution layer is made of five 7 × 7 filters. Take the CNN full-size (128 × 20) input for example. The convolved images are of size (128−7+1, 20−7+1, 5), i.e., (122, 14, 5) and the one resulted from the kth ($k = 1, \ldots, 5$) filter, $\mathbf{W^k}$, can be described by

$$\mathbf{h}_{ij}^{k} = \varphi((\mathbf{W}^{k} * \mathbf{X})_{ij} + b) \quad i = 1, \ldots, 122, \quad j = 1, \ldots, 14 \tag{1}$$

where $\mathbf{X}$ and b are the input image and the bias. The convolution operation is denoted by $*$ and the activation function by φ. The widely adopted rectified linear unit is chosen for φ, that is,

$$\varphi(z) = \max(0, z). \tag{2}$$

The max pooling layer is of pooling size (2, 2) and stride (step size) 2 [9]. This layer preserves the max value of every nonoverlapped 2 × 2 block in the feature map to generate a subsampled one of size (122/2, 14/2, 5), i.e., (61, 7, 5). The first fully connected layer is thus of dimension 2315 (= 61 × 7 × 5). The second fully connected layer is equipped with three units, and this value is taken according to [7] for later comparison of complexity between CNN and NN. The structure and functionality of fully connected layers are quite similar with those of the hidden layers in NNs, and for conciseness, find detailed formulations in [7].

For sea ice detection (classification model), the output layer is designed with two units a_1 and a_2, and the activation

function is the softmax function, which gives the probability of occurrence of sea ice or seawater

$$p_r = \frac{\exp(a_r)}{\sum_{s=1}^{2} \exp(a_s)}, \quad \text{where } r = 1, 2. \tag{3}$$

The detection result is based on the one with higher value.

For SIC estimation purposes (regression model), the output layer shown in Fig. 1 is modified to have one unit (i.e., the concentration value), and a linear activation function is adopted

$$f(z) = z. \tag{4}$$

It should also be noted that the overall layout of CNNs remains the same when a cropped DDM is used as input, only the size of each layer needs to be adjusted accordingly and this can be readily deduced following the above-mentioned procedure and has been given in Fig. 1 as set B.

C. CNN Training

Back-propagation learning [13] and minibatch stochastic gradient descendant with momentum (SGDM) algorithm [14] are adopted for training. The learning method includes a forward propagation and a backward propagation. The forward propagation hereafter is denoted by F, during which the parameters are all fixed. During the backward propagation, SGDM updates the parameters by slowly progressing in the direction of the negative gradient of the cost function to minimize the cost. The cost function over a minibatch (whose size is arbitrarily chosen as 100 in this letter) is given as

$$\varepsilon(F(\mathbf{X}; \mathbf{W}), \mathbf{y}) = \frac{1}{100} \sum_{n=1}^{100} (F(\mathbf{X}_n; \mathbf{W}) - \mathbf{y}_n)^2 \tag{5}$$

where the nth input and output within the minibatch are denoted by $\mathbf{X}_n$ and $\mathbf{y}_n$. The parameters are updated over every minibatch of the training data iteratively, through [14]

$$\begin{aligned} \mathbf{V}_{q+1} &= m \cdot \mathbf{V}_q - \eta \cdot \left\langle \frac{\partial \varepsilon}{\partial \mathbf{W}}\bigg|_{\mathbf{W}_q} \right\rangle \\ \mathbf{W}_{q+1} &= \mathbf{W}_q + \mathbf{V}_{q+1} \end{aligned} \tag{6}$$

where q is the iteration index, $\mathbf{V}$ is the momentum variable, $\langle (\partial \varepsilon / \partial \mathbf{W})|_{\mathbf{W}_q} \rangle$ is the average over the qth batch of the derivative evaluated at $\mathbf{W}_q$, the learning rate η is set as 0.001, and the momentum m as 0.95. Here, a scheme of epoch training [14] is selected. An epoch means a full pass over all minibatches.

In summary, a minibatch SGDM-based back-propagation learning for filter parameters is conducted as follows.

1) Initialize $\mathbf{W}$ with random numbers (Gaussian distributed with mean 0 and standard deviation 0.01) and present all the training data (input and target) to the network.
2) Proceed forward propagation F and compute the cost function using (5).
3) Update $\mathbf{W}$ using (6).
4) This training process stops when:
   a) the preset maximum number (50) of epochs is reached; or
   b) the changes in cost function are less than 0.001 among 10 consecutive epochs.

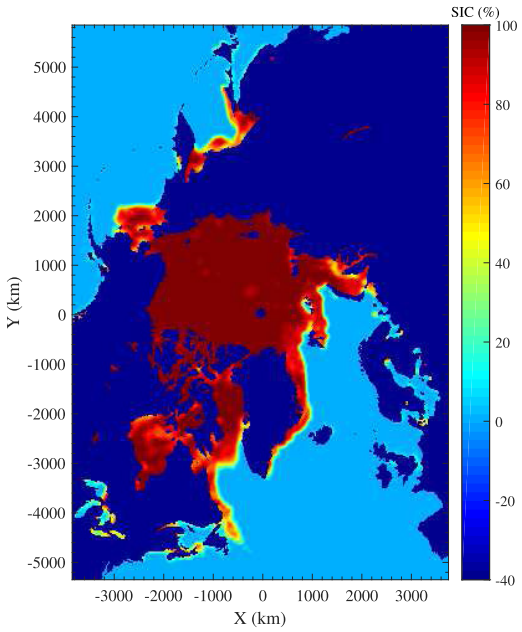

Fig. 3. Example of the reference SIC data were from passive microwave sensors [15]. The SIC value ranges from 0% to 100%. For better illustration, the land and the region without data are set with a value of −40.

III. Experiments

A. Data

To facilitate the performance comparison between the proposed CNN-based and the existing NN-based sea ice remote sensing methods, the same DDM data sets from [7] were employed. Specifically, training samples were collected from February 3–5, 2015 with an identifier receiver data (RD) 17 and the employed track ID [track data (TD)] can be found in [7]. Note that a DDM data set can be uniquely determined given both RD and TD. The test data sets were from RDs 18, 19, 23, and 27 collected during February 11–13, February 19–21, March 15–17, and April 16–18, 2015, respectively.

The reference SIC data were collected by the Nimbus-7 Scanning Multi-Channel Microwave Radiometer and Defense Meteorological Satellite Program Special Sensor Microwave Imager-Special Sensor Microwave Imager/Sounder passive microwave sensors [15] (see Fig. 3 for an example of such data on April 17, 2015). The SIC data can be associated with a DDM image based on the same collection period (within the same day) and the collocated measured region. The SIC data were modified to approximate the illuminated region of a DDM image, by averaging each pixel (of resolution 25×25 km^2) with its adjacent 5×5 grids, and the averaged data were regarded as ground truth here. For SIC estimation, the target data were the ground truth. For sea ice detection, the target output was labeled as "sea ice" if the ground-truth SIC was above 5%, otherwise it was identified as "seawater." This threshold was selected based on the minimum detectable SIC from DDMs, which was found to be 5% [7].

B. Results and Evaluation

The SIC estimation- and sea ice detection-orientated CNNs were trained and tested using the same data as those in [7], and the results are tabulated in Tables I and II, in which the

TABLE I
ERROR STATISTICS FOR SIC ESTIMATION USING DIFFERENT INPUT SIZES

ID	Collection period	Numbers	Full-size input				Cropped input			
			E_{std}		R		E_{std}		R	
			CNN	NN	CNN	NN	CNN	NN	CNN	NN
RD 17 (training)	Feb. 03 to 05, 2015	8377	0.15	0.11	0.95	0.97	0.15	0.11	0.95	0.97
RD 18 (test)	Feb. 11 to 13, 2015	6071	0.17	0.20	0.91	0.88	0.16	0.17	0.92	0.91
RD 19 (test)	Feb. 19 to 21, 2015	4915	0.15	0.17	0.93	0.92	0.15	0.16	0.94	0.93
RD 23 (test)	Mar. 15 to 17, 2015	4799	0.16	0.19	0.93	0.91	0.15	0.13	0.94	0.95
RD 27 (test)	Apr. 16 to 18, 2015	8522	0.18	0.20	0.89	0.86	0.17	0.18	0.89	0.90
		Average	0.16	0.17	0.92	0.91	0.16	0.15	0.93	0.93

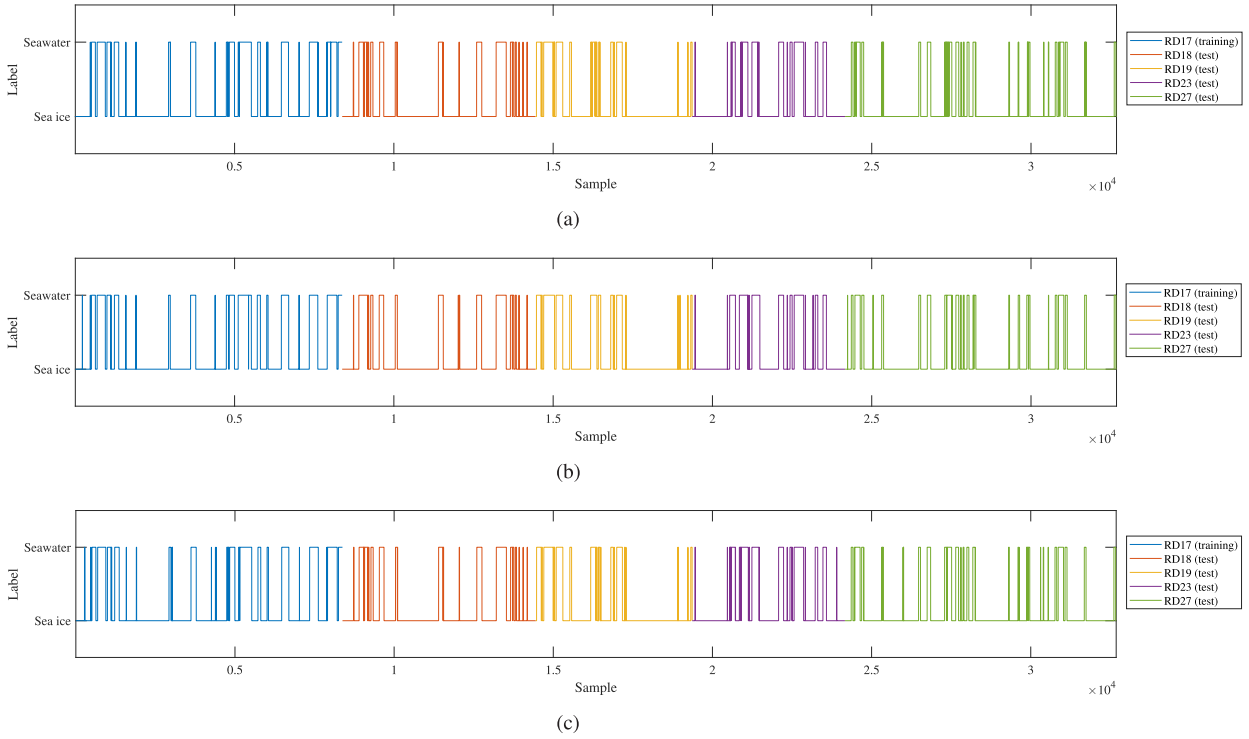

Fig. 4. Sea ice detection results. (a) Ground-truth data. (b) Output from full-size input. (c) Estimation resulting from cropped input.

TABLE II
ACCURACY OF ICE DETECTION

ID	Full-size input		Cropped input	
	CNN	NN	CNN	NN
RD 17 (training)	99.15%	99.60%	99.03%	99.13%
RD 18 (test)	98.12%	97.94%	98.94%	99.01%
RD 19 (test)	97.97%	97.29%	98.77%	98.54%
RD 23 (test)	96.42%	93.98%	98.41%	98.04%
RD 27 (test)	97.04%	95.97%	98.43%	98.41%
Average	97.83%	97.17%	98.73%	98.67%

outcomes resulting from the full-size and cropped inputs are both presented. For illustration, the sea ice detection results are also shown in a sample-by-sample manner in Fig. 4. For the SIC evaluation, the standard deviation error E_{std} and the correlation coefficient R between the estimation and ground truth were derived, and they are given as [7]

$$E_{\text{std}} = \text{std}(\text{SIC}_{\text{cnn}} - \text{SIC}_{\text{ref}})$$
$$R = \frac{\text{cov}(\text{SIC}_{\text{cnn}}, \text{SIC}_{\text{ref}})}{\text{std}(\text{SIC}_{\text{cnn}})\text{std}(\text{SIC}_{\text{ref}})}. \quad (7)$$

As shown in Tables I and II, the proposed CNN-based sea ice remote sensing shows the overall improved accuracy over the existing NN-based one, especially when using the original input size. It can be noted that the differences between the results of these methods are quite small. Thus, the standard error (which is the ratio of sample standard derivation over the square root of the effective number of independent samples) in the estimates of the statistics is calculated. Note that every TDS-1 DDM sample is independent of each other. The standard errors of E_{std} were found to be from 0.0016 to 0.0022 and those for R were in the order of 10^{-4}. Thus, the CNN-based method outperforms the NN-based method.

An advantage of CNN lies in the usage of filters in the convolution layer, which appeared to be able to reduce the noise in the DDM. The deployment of the convolution and pooling layers makes CNN less sensitive to the disalignment of the DDM specular point within a frame. Note that a pooling layer of size (2, 2) and stride 2 is able to resolve 1-pixel fluctuation. The resistance to the unsettlement relies on the depth and size of the convolution and pooling layers. Since only one layer of each was adopted in this letter, the ability of the designed CNN to be completely independent of the data locations is quite limited. This also accounts for the varied

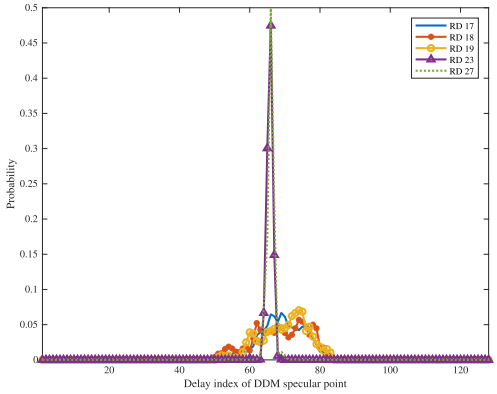

Fig. 5. Probability density distribution of the delay pixel index for DDM specular point for each data set.

precision among different data sets since the degree of fluctuation differs (see Fig. 5 for the probability density distribution of the delay pixel index for the DDM specular point). In Fig. 5, obvious discrepancies can be found between the training set RD 17 and test sets RDs 23 and 27, and this could result in the drop of sea ice sensing accuracy from using the cropped data to full-size ones (for both CNN and NN). However, CNN still outperforms NN with the original DDM format as discussed earlier and its performance may be further enhanced with more layers. When the data are adequately processed by cropping the DDM for alignment, both CNN and NN can produce a good result.

In addition to the advancement in accuracy, the designed CNNs are with fewer parameters than NNs for the same task, which makes the training easier [9]. For illustration, the sea ice detection-orientated CNN has 6666 $(= (7 \times 7 + 1) \times 5 + (2315 + 1) \times 3 + (3 + 1) \times 2)$ parameters, while the NN has 7691 $(= (128 \times 20 + 1) \times 3 + (3 + 1) \times 2)$ for full-size input; and those for cropped images are 2046 and 2411, respectively.

IV. Conclusion

In this letter, the technique of CNN is applied to sea ice remote sensing using TDS-1 DDM data. Classification-based and regression-based networks were designed for sea ice detection and SIC estimation, respectively. In addition, the networks were evaluated using both full-size and cropped DDM images. The devised scheme was found to be better than the current NN-based one in terms of: 1) overall improved accuracy; 2) fewer parameters in the network (easier to train); and 3) more tolerant to changes in the input data structure (requires less data preprocessing, without the need for registering the delay coordinate of the specular point). In the future, more layers can be introduced and more training samples should be involved to further improve the accuracy. In order to maintain a good spatial resolution of TDS-1 DDM, no extra noncoherent summation over DDM is applied in this letter, but this process is worth trying to mitigate the speckle noise to enhance the performance in the future.

References

[1] O. M. Johannessen *et al.*, *Remote Sensing of Sea Ice in the Northern Sea Route*. Chichester, U.K.: Praxis, 2007.
[2] Q. Yan and W. Huang, "Spaceborne GNSS-R Sea ice detection using delay-Doppler maps: First results from the U.K. TechDemoSat-1 mission," *IEEE J. Sel. Topics Appl. Earth Observ. Remote Sens.*, vol. 9, no. 10, pp. 4795–4801, Oct. 2016.
[3] Y. Zhu, K. Yu, J. Zou, and J. Wickert, "Sea ice detection based on differential delay-Doppler maps from UK TechDemoSat-1," *Sensors*, vol. 17, no. 7, p. 1614, 2017.
[4] A. Alonso-Arroyo, V. U. Zavorotny, and A. Camps, "Sea ice detection using U.K. TDS-1 GNSS-R data," *IEEE Trans. Geosci. Remote Sens.*, vol. 55, no. 9, pp. 4989–5001, Sep. 2017.
[5] D. Schiavulli, F. Frappart, G. Ramillien, J. Darrozes, F. Nunziata, and M. Migliaccio, "Observing sea/ice transition using radar images generated from TechDemoSat-1 delay Doppler maps," *IEEE Geosci. Remote Sens. Lett.*, vol. 14, no. 5, pp. 734–738, May 2017.
[6] A. Rius *et al.*, "Feasibility of GNSS-R ice sheet altimetry in greenland using TDS-1," *Remote Sens.*, vol. 9, no. 7, p. 742, 2017.
[7] Q. Yan, W. Huang, and C. Moloney, "Neural networks based sea ice detection and concentration retrieval from GNSS-R delay-Doppler maps," *IEEE J. Sel. Topics Appl. Earth Observ. Remote Sens.*, vol. 10, no. 8, pp. 3789–3798, Aug. 2017.
[8] L. Zhang, L. Zhang, and B. Du, "Deep learning for remote sensing data: A technical tutorial on the state of the art," *IEEE Geosci. Remote Sens. Mag.*, vol. 4, no. 2, pp. 22–40, Jun. 2016.
[9] L. Wang, K. A. Scott, L. Xu, and D. A. Clausi, "Sea ice concentration estimation during melt from dual-pol SAR scenes using deep convolutional neural networks: A case study," *IEEE Trans. Geosci. Remote Sens.*, vol. 54, no. 8, pp. 4524–4533, Aug. 2016.
[10] X. Shen *et al.*, "Sea ice classification using Cryosat-2 altimeter data by optimal classifier–feature assembly," *IEEE Geosci. Remote Sens. Lett.*, vol. 14, no. 11, pp. 1948–1952, Nov. 2017.
[11] X. X. Zhu *et al.*, "Deep learning in remote sensing: A comprehensive review and list of resources," *IEEE Geosci. Remote Sens. Mag.*, vol. 5, no. 4, pp. 8–36, Dec. 2017.
[12] G. Foti *et al.*, "Spaceborne GNSS reflectometry for ocean winds: First results from the UK TechDemoSat-1 mission," *Geophys. Res. Lett.*, vol. 42, no. 13, pp. 5435–5441, Jul. 2015.
[13] P. Werbos, "Beyond regression: New tools for prediction and analysis in the behavioral sciences," Ph.D. dissertation, Committee Appl. Math., Haivard Univ., Cambridge, MA, USA, Nov. 1974.
[14] Y. LeCun, L. Bottou, G. B. Orr, and K.-B. Müller, "Efficient backprop," in *Neural Networks: Tricks of the Trade*. Berlin, Germany: Springer-Verlag, 2012, pp. 9–48.
[15] D. J. Cavalieri, C. Parkinson, P. Gloersen, and H. J. Zwally, "Sea ice concentrations from Nimbus-7 SMMR and DMSP SSM/I passive microwave data," Nat. Snow Ice Data Center, Boulder, CO, USA, 1996.